FDTD Modeling of Scattered Ultra-Low Frequency Electromagnetic Waves From Objects Submerged in the Ocean

Dallin R. Smith, *Student Member, IEEE*, Sean Burns, Jamesina J. Simpson, *Senior Member, IEEE*, and Stephanie M. Ferrone

***Abstract*— The skin depth of electromagnetic (EM) waves in ocean water is on the order of 160 m at 3 Hz and just 50 m at 30 Hz. The detection of objects in the ocean using EM waves is, thus, very challenging due to the high attenuation rate of the EM fields. We propose the usage of ultra-low frequencies (ULF: <3 Hz) to detect submerged objects due to the larger skin depths (1.5 km at 0.03 Hz) at those frequencies. Using the finite-difference time-domain (FDTD) method, ULF scatterings from objects submerged in the ocean are obtained. This is achieved by running the FDTD model in the scattered-field-only regime, in which EM field components in a 3-D FDTD grid are excited by a "hard" source, i.e., the electric field components are set to a sinusoid at ULF to represent the scatterings from the object. The propagation attenuation versus distance from the source (object) is recorded and compared to the propagation attenuation as predicted by the plane wave theory. A total round-trip propagation attenuation is estimated for ULF waves originating in the air region above the ocean. Frequencies ranging from 0.01 to 2 Hz are tested.**

***Index Terms*— Airplane, earth, electromagnetic (EM) propagation, extremely low frequency (ELF), finite-difference time-domain (FDTD) method, ocean, ultra-low frequency (ULF).**

I. Introduction

LOCATING and detecting objects submerged in the ocean have been of interest for many decades. For example, submerged aircrafts are of interest in part due to the disappearance of Malaysia Airline Flight MH370 in March of 2014, which initiated a search mission that lasted for months and entailed a survey of 120 000 km^2 of the sea floor near Southeast Asia [1]. The multinational search efforts for this aircraft were the largest and most expensive in aviation history [2], and the aircraft was never found.

In some cases, sonar may be used when the object of interest is sufficiently noisy. Alternatively, over short ranges, magnetic anomaly detectors may be employed [3]. In general, electromagnetic (EM) waves are not a viable option due to the high attenuation rate within the conductive ocean water. Using the plane-wave theory, the expected skin depth at extremely low frequencies (ELFs: 3 Hz–3 kHz) is just 50 m at 30 Hz and 160 m at 3 Hz. Ronald and King [4] provide the analytical calculations for the localized detection of relatively shallow (100 m) conducting cylinders in the ocean at ELF. EM waves scattering from objects at much greater depth would not be detectable by the time they reached the ocean surface.

Rather than using ELF or higher frequency waves, we propose a radar system that employs ultra-low frequency (ULF: <3 Hz) EM waves to detect objects in the ocean, such as downed aircrafts. The skin depth of an ULF EM plane wave in ocean water is 276 m at 1 Hz and 872 m at 0.1 Hz. Note that the average depth of the ocean is 3.55 km [5]. Specifically, the proposed ULF radar system involves three steps.

1) Generate a worldwide ULF EM field that penetrates into every ocean.
2) Establish baseline values of the ULF EM field at and above the ocean surface at points of interest using the previous measurement data obtained before the addition of the submerged aircraft or using gradiometry.
3) Detect in real-time perturbations of the ULF EM field generated by the objects of interest submerged at depths at the positions of interest.

The focus of this paper is on the propagation of ULF waves in the earth–ionosphere waveguide, along with the total round-trip attenuation of ULF waves from the surface of the ocean, down to the object of interest, and then back up to the surface of the ocean. The best strategies to generate the ULF waves in the earth–ionosphere waveguide (Step 1) will be considered in future work. Man-made sources of ULF waves already exist today, such as the high-frequency active auroral research program (HAARP) in Alaska and other similar facilities [6], [7]. There are also natural sources of ULF waves such as those due to resonances in the magnetospheric cavity and the interaction of solar particles and radiative pressure with the magnetosphere [8], [9].

In Section II, the global propagation of ULF waves is discussed along with the high degree of refraction that is experienced by these waves at the ocean surface, resulting in a vertically downward-propagating ULF plane wave into

Manuscript received September 12, 2017; revised November 9, 2018; accepted December 9, 2018. Date of publication January 8, 2019; date of current version April 5, 2019. This work was supported in part by the Office of Naval Research under Grant N00014-15-1-2283. *(Corresponding author: Dallin R. Smith.)*

D. R. Smith, S. Burns, and J. J. Simpson are with the Electrical and Computer Engineering Department, University of Utah, Salt Lake City, UT 84112 USA (e-mail: dallinsmith9@gmail.com).

S. M. Ferrone is with the Office of Naval Research, Arlington, VA 22217 USA.

Color versions of one or more of the figures in this paper are available online at http://ieeexplore.ieee.org.

Digital Object Identifier 10.1109/TAP.2019.2891464

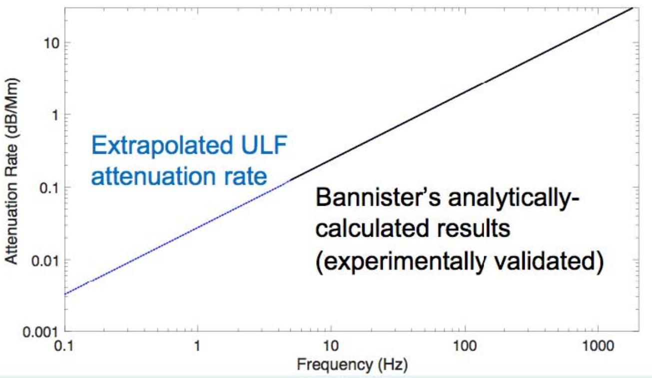

Fig. 1. Extrapolation of Bannister's analytically calculated and experimentally validated ELF attenuation rate in the earth–ionosphere waveguide (black line) [7] to ultra-low frequencies (blue line).

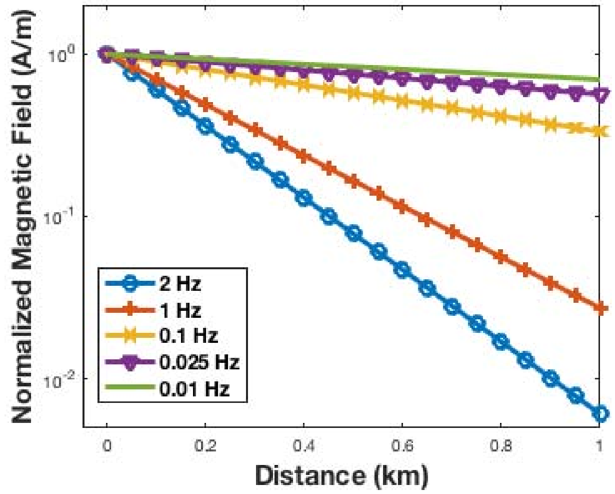

Fig. 2. Attenuation of the ULF plane wave propagating nearly vertically downward from the surface of the ocean down to the object of interest.

the ocean. Section III provides the plane-wave theory results for the attenuation of the ULF waves from the ocean surface to the depth of the object. Section IV describes the all-ocean finite-difference time-domain (FDTD) [10], [11] model (called "Model #1) used to calculate the attenuation rate of the scattered EM fields back up to the ocean surface. The results from Model #1 are provided in Sections V. Section VI includes a convergence study of the FDTD grid resolution and geometry of the object. Section VII describes a second FDTD model that includes the ocean, atmosphere, and lower ionosphere (called "Model #2"). Sections VIII, IX, and X provide the results for Model #2. This paper then concludes with a discussion of the background noise level at ULF (Section XI), detection methods of the scattered ULF wave (Section XII), and concluding remarks (Section XIII).

II. Global ULF Waves Incident on Ocean Surfaces

ULF waves can propagate globally in the earth–ionosphere waveguide with negligible attenuation, as shown in Fig. 1. In Fig. 1, the analytically calculated and experimentally confirmed attenuation rate of ELF waves in the earth–ionosphere waveguide is illustrated [12]. These results are extrapolated down to ULF. As can be seen in Fig. 1, the attenuation rate at 0.1 Hz is approaching 0.001 dB/Mm. Thus, any impinging ULF wave generated by a man-made source in the earth–ionosphere is expected to be of the same approximate amplitude at the surface of any ocean around the world.

These ULF waves that propagate in the earth–ionosphere waveguide propagate as quasi-transverse EM (TEM) waves between two conducting spheres: the bottom side of the ionosphere and the ocean/lithosphere surface. The ULF waves are locally not exact TEM waves due to the varying ionosphere composition and topography.

Since the propagating ULF waves in the earth–ionosphere waveguide are not exact TEM waves, a portion of the quasi-TEM ULF wave will be incident on the ocean surface at an angle of less than 90°. Due to a high degree of refraction at the ocean surface, the ULF wave will propagate nearly vertically downward as a plane wave into the ocean. For example, a plane-wave incident on an ocean surface (relative permittivity, $\varepsilon_r = 81$, conductivity, $\sigma = 3.3$ S/m, relative permeability, $\mu_r = 1$, and frequency, f = 0.1 Hz) at an angle of 89° will propagate nearly vertically downward at an angle of 0.0001° according to Snell's Law. As a result, any ULF wave propagating into the ocean from the air will be a plane wave propagating nearly directly vertically (radially) downward into the ocean.

III. Attenuation of the Downward Propagating Wave

Since the ULF wave just below the ocean surface is a plane wave propagating nearly vertically downward, the attenuation rate may be calculated using the plane-wave theory. Fig. 2 shows the plot of the attenuation of the normalized electric and magnetic field components of plane waves at frequencies ranging from 0.01 to 2 Hz. The amplitude of a 0.1 Hz plane wave is seen to drop by a factor of less than 10:1 upon reaching a depth of 1 km.

IV. All-Ocean FDTD Model ("Model #1") Description

FDTD modeling is used to calculate the attenuation rate of the ULF waves scattered by the object of interest and propagating back up to the ocean surface. A full-vector Maxwell's equation solution is required in this case because at ULF, the entire region from the scattering object to the surface of the ocean is in the near field of the object. The EM wavelength in the ocean at 0.1 Hz is 5.48 km.

The 3-D Cartesian-coordinate FDTD models were used in a scattered-field-only mode [13] in order to obtain the attenuation rate of EM waves scattered off an isolated aircraft submerged 1 km deep in the ocean. In this model, the aircraft is modeled as a source in the FDTD grid, with a sinusoidal time waveform. A variety of ultra-low frequencies are tested in separate FDTD simulations.

The *z*-direction corresponds to the vertical direction, and the *x*- and *y*-directions correspond to the longitude and latitude directions, respectively. For this paper, the entire grid is set to ocean water ($\varepsilon_r = 81$, $\sigma = 3.3$ S/m, and $\mu_r = 1$).

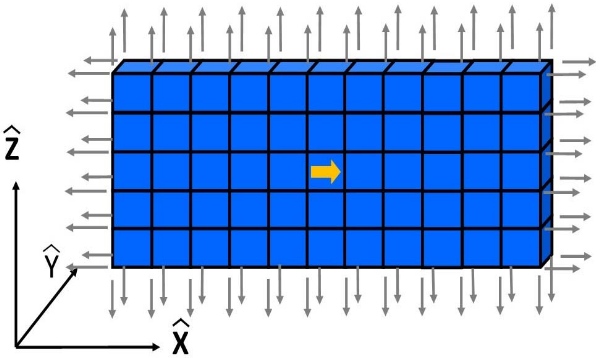

Fig. 3. Zoomed-in view of the geometry of the source modeled along an E_x component in the 3-D FDTD grid of ocean water. Yellow arrow: electric field along the x-direction set to the source waveform. Blue cells: grid cells set to ocean water ($\sigma = 3.3$ S/m, $\varepsilon_r = 81$, and $\mu_r = 1$) extending away from the source region to the edges of the grid (not shown) in all three Cartesian directions.

A 60 m grid resolution is employed and the grid extends out to 6 km (at which distance the scattered fields have decayed sufficiently to zero so as to not introduce any reflections back into the grid).

A time step increment of 99% of the Courant stability limit is utilized [14]. Additional simulations demonstrated that the initial peak obtained at the first quarter of a wavelength of the sinusoidal signal corresponds to the steady-state amplitude due to the long wavelengths at ULF and short time step increment. A perfect electric conductor (PEC) boundary condition is implemented on all sides of the grid since the grid is large enough for the waves to attenuate before reaching the edges of the grid.

The source was positioned as a single cell of the electric field component in the x-direction: E_x, which represents scattering off an aircraft that is 60 m long. The effective size of the object is 60 m on each side. (Additional simulations indicated that the attenuation away from the aircraft was dominated by the length of the source and not the diameter.) The grid geometry in the vicinity of the source is shown in Fig. 3.

V. Attenuation of the Upward Propagating Wave

Using Model #1 (the 60 m FDTD grid of Section IV), the attenuation rate of the upward propagating scattered ULF wave is calculated from an aircraft of diameter ~60 m and of length 60 m. Fig. 4 illustrates the magnetic field attenuation at different frequencies, where 0 km along the z-axis (horizontal axis shown in Fig. 4) corresponds to the position of the aircraft. Fig. 5 provides a zoomed-in view of Fig. 4 that extends along the z-axis only out to 1 km.

In Fig. 5, a frequency of 0.1 Hz appears to be an ideal frequency up to a distance of 1 km because frequencies below 0.1 Hz do not yield a significant improvement in the magnetic field attenuation. Furthermore, it is advantageous to use a frequency as high as possible, since lower frequencies correspond to even longer wavelengths and antenna sizes. At 0.1 Hz, the magnetic field drops by ~1000:1 over a distance of 1 km.

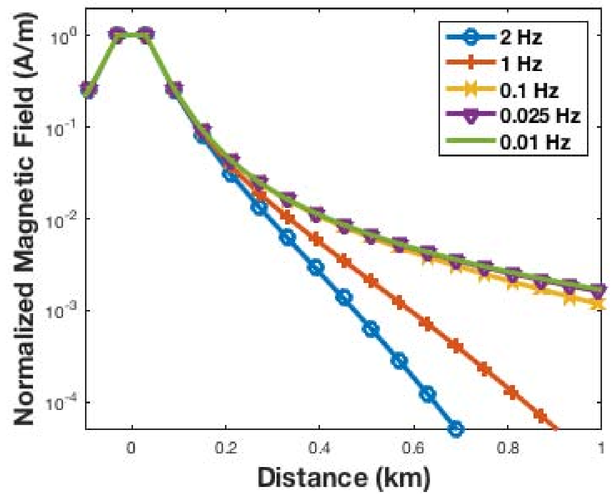

Fig. 4. Attenuation of the H_y components of the scattered ULF wave from the aircraft of Fig. 3 at 2, 1, 0.1, 0.025, and 0.01 Hz.

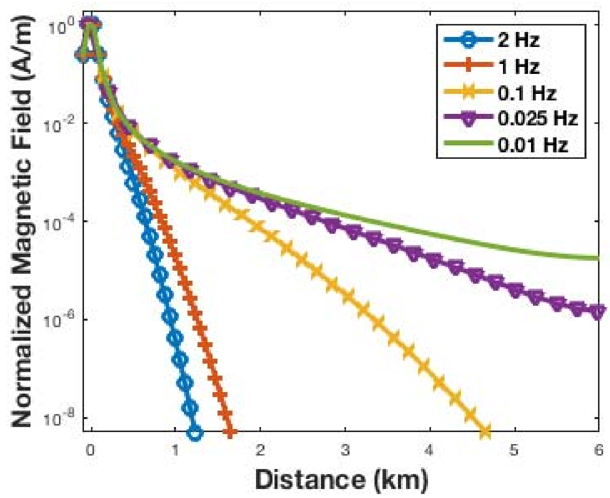

Fig. 5. Zoomed-in view of Fig. 4 (plotted out to 1 km).

Fig. 6 shows the comparison of the results at 0.1 Hz of Fig. 5, along with the corresponding E_x attenuation away from the scattering aircraft. In Fig. 6, it is observed that the electric and magnetic fields attenuate at different rates. (They do not constitute a plane wave, which is expected in the near-field region of the scattering aircraft.) The magnetic fields attenuate more slowly than the electric fields, so it would be advantageous to measure the magnetic fields scattered from a submerged aircraft rather than electric fields.

Fig. 6 also shows the plane-wave attenuation result from Fig. 2 at a frequency of 0.1 Hz. Fig. 6 shows that there is a substantial difference between the near-field (upward propagating) FDTD calculated electric and magnetic field attenuations versus the (downward propagating) plane-wave theory result.

Another consideration is the length of the scattering object of interest. Using the same model (Model #1), various object (i.e., source) sizes were tested while keeping a constant object diameter of 60 m. Fig. 7 illustrates the attenuation rate for

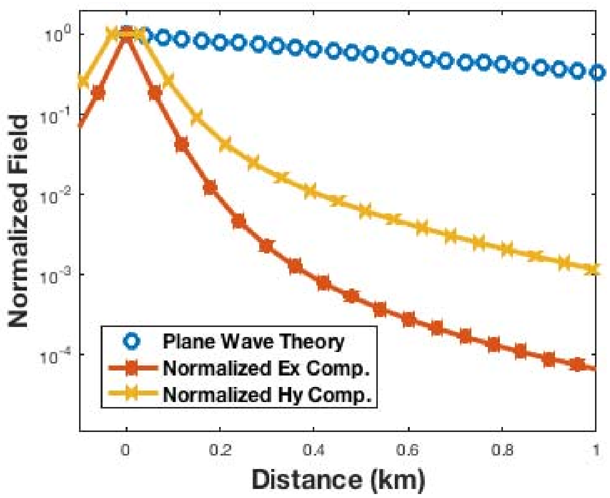

Fig. 6. Comparison of the FDTD-calculated normalized E_x and H_y components along the *z*-direction away from the 60 m-diameter and 60 m-long aircraft at a frequency of 0.1 Hz. For comparison, the plane-wave theory attenuation result at 0.1 Hz in Fig. 2 is shown.

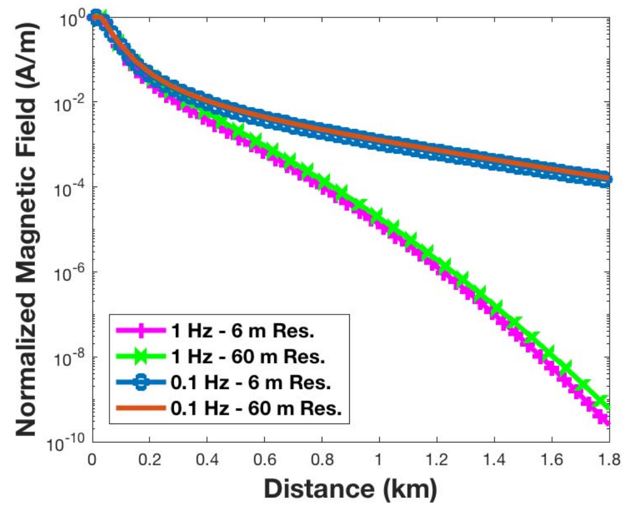

Fig. 8. Comparison of the magnetic field attenuation away from the 60 m-diameter and 60 m-long scattering aircraft modeled in an FDTD grid at 60 m versus 6 m grid resolution for 0.1 and 1 Hz sources.

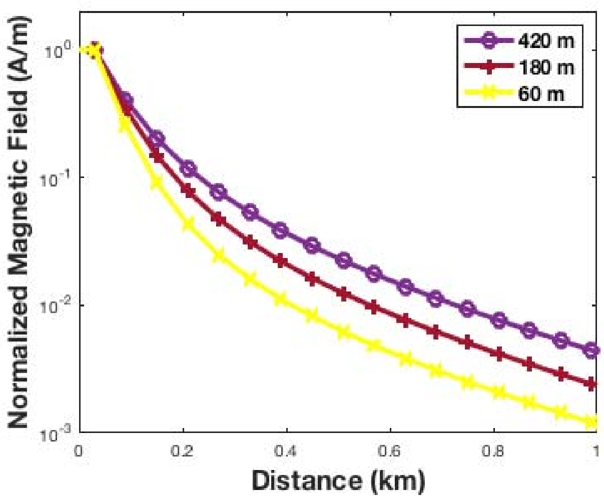

Fig. 7. Comparison of the attenuation rate away from submerged objects of different lengths ranging from 60 to 420 m. A source frequency of 0.1 Hz was used, and the object diameter was kept at 60 m.

different object sizes ranging from 60 to 420 m. A source frequency of 0.1 Hz was used in all three cases. The magnetic fields are seen to attenuate more slowly away from a longer aircraft than a shorter aircraft.

VI. Convergence Test

A convergence test was simulated to test the object size and grid resolution. To test for convergence and to verify the size of the scattering aircraft that is modeled in the grid, an analogous FDTD simulation to that of Model #1 is run at a resolution of 6 m (10 times higher resolution in all three Cartesian directions). A correspondingly smaller time step (99% of the Courant limit) is required for the higher resolution test. As a result, the simulation time is lengthened by both the grid size and the required time step. Source frequencies of 0.1 and 1 Hz were used.

For the 6 m resolution case, the source is modeled along a series of electric field components ten cells long in the x-direction, yielding a total length of 60 m. In the cross-sectional direction (i.e., the yz plane), E_x components within a circle of diameter 60 m are set to the source. For the 60 m resolution case, the source is a single E_x components of length 60 m and of diameter 60. Thus, both models set to different grid resolutions have the same effective source size.

Fig. 8 shows the comparison of the 60 m resolution results at 0.1 and 1 Hz from Fig. 4 to the 6 m resolution results. Good agreement is obtained between the two results at both frequencies, indicating that a coarser 60 m resolution may be used to provide sufficiently accurate results using a much shorter and smaller simulation.

VII. Ocean–Ionosphere Model Description

To better understand the behavior of the scattered ULF EM fields at the ocean–air boundary and in the atmosphere, a second FDTD model is generated that includes the atmosphere and lower ionosphere (called Model #2). The scattering aircraft is placed at a depth of 1 km within the ocean. To keep the size and length of the simulation reasonable, a frequency of 1 Hz is used as the source frequency. A grid resolution of 60 m is employed, and the total grid size is 800 × 800 × 1725 cells along the x-, y-, and z-directions, respectively. The ocean is modeled in the first 50 cells in the z-direction, constituting a depth of 3 km (close to the average depth of the ocean [5], and 3 km which sufficiently attenuate the ULF wave at 1 Hz). The remaining 1675 cells model the atmosphere and lower ionosphere up to an altitude of 100.5 km. The ionosphere is modeled using a daytime exponential conductivity profile according to [15]. Specifically, Equation (1) is the conductivity (σ) profile measured in S/m that is used to model the ionosphere, where z is the altitude in kilometers

$$\sigma = \left(2.5\times10^{5}\right) \mathrm{Exp}\left[0.3\left(z-70\right)\right]. \tag{1}$$

For this simulation, a PEC boundary condition is implemented on the top and bottom edges of the grid. A perfectly matched layer (PML) is used to terminate the air region of

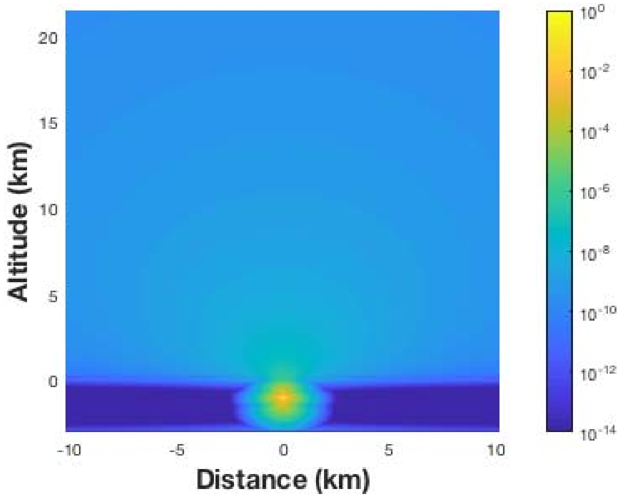

Fig. 9. Zoomed-in view of a 2-D slice of E_x component normalized in the 3-D FDTD grid of Model #2. The surface of the ocean corresponds to an altitude of 0 km. The source is at an altitude of −1 km (a depth of 1 km in the ocean) and horizontally at 0 km. The scale bar is in units of V/m.

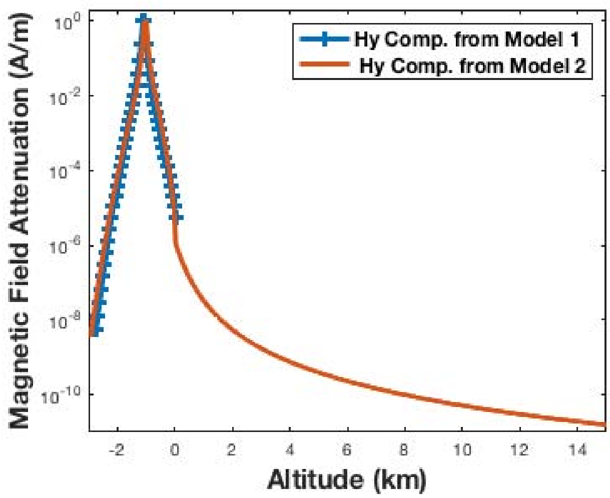

Fig. 10. Comparison of the normalized magnetic fields as a function of altitude in Model #1 (all ocean) versus Model #2 (ocean + atmosphere + lower ionosphere). A common axis is used for both plots (source location at an altitude of −1 km).

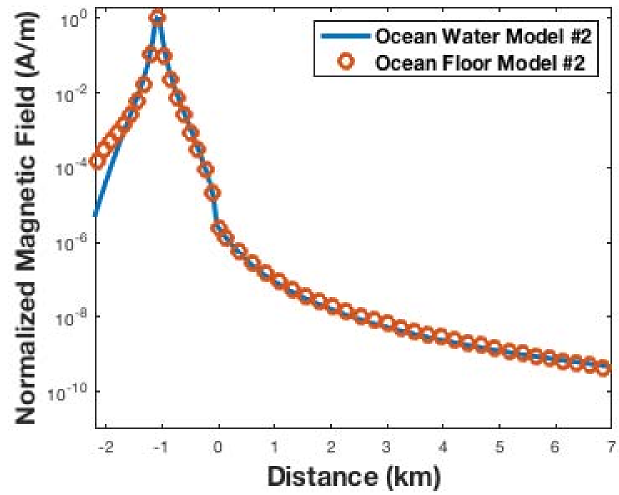

Fig. 11. Blue line is the normalized magnetic field of original Model #2 with the ocean water below the aircraft as shown in Fig. 10. It is compared with new Model #2 with the lithosphere (ocean floor) directly below the aircraft. This figure is a zoomed-in view ranging from −2 to 7 km.

the grid in the x- and y-directions. (No PML is needed in the z-direction due to the conductive ocean and ionosphere which sufficiently attenuates that the ULF waves before the edges of the grid are reached.) PML is 100 cell thick because the grid cell dimensions are quite small (60 m) in the air region relative to a wavelength (300 Mm at 1 Hz).

VIII. Ocean–Ionosphere Model Results

Fig. 9 shows a screenshot after 0.25 s of the outward propagating wave from the scattering aircraft. Note that Fig. 9 shows a zoomed-in view of the entire grid, which extends up to an altitude of 100 km and to 24 km on either side of the source. The wave is seen to propagate farther and faster in the air region than in the ocean water.

Fig. 10 shows a zoomed-in view (up to an altitude of 15 km) of the normalized magnetic field attenuation away from the scattering aircraft. In this case, 0 km along the z-axis (horizontal axis shown in Fig. 10) corresponds to the surface of the ocean rather than the location of the aircraft as in Figs. 4–8. The scattering aircraft is at an altitude of −1 km. The upward propagation ULF wave is reflected at the ocean–atmosphere interface due to the high conductivity contrast. This generates an evanescent wave above the ocean surface. Since the wavelength at the ULF is large, these evanescent waves extend substantially into the air region as shown in Fig. 10. Also, due to the change in material parameters, the amplitude of the ULF field decreases by about an order of magnitude across the ocean surface at 0 km.

For comparison, the ocean-only result of Fig. 4 at 1 Hz is also included in the plot (but shifted so it is centered at an altitude of −1 km to correspond to the location of the source in Model #2). The attenuation within the ocean is nearly identical between Models #1 (ocean only) and #2 (ocean + atmosphere + lower ionosphere).

IX. Impact of the Ocean Floor

The effect of the ocean floor is now studied. Model #2 is rerun with the aircraft at a depth of 1 km below the ocean surface as before in Section VII. This time, however, the ocean floor is placed directly below the aircraft (rather than having more ocean water below it). Twenty cells (1.2 km) of lithosphere ($\sigma = 0.001$ S/m and $\varepsilon_r = 15$) are directly modeled below the aircraft in the FDTD grid. A surface impedance boundary condition (SIBC) is applied at the bottom edge below the lithosphere [16]. Begg's method is used to formulate SIBC [17].

Fig. 11 presents the original results from Model #2 (as shown in Fig. 10 for more ocean water below the aircraft) along with the new results for the case of sea floor (lithosphere) below the aircraft. As seen in Fig. 11, the fields above the aircraft are virtually identical whether there is ocean below the aircraft or a sea bed. This same effect is observed in Fig. 10. The presence of the ocean–air interface does not

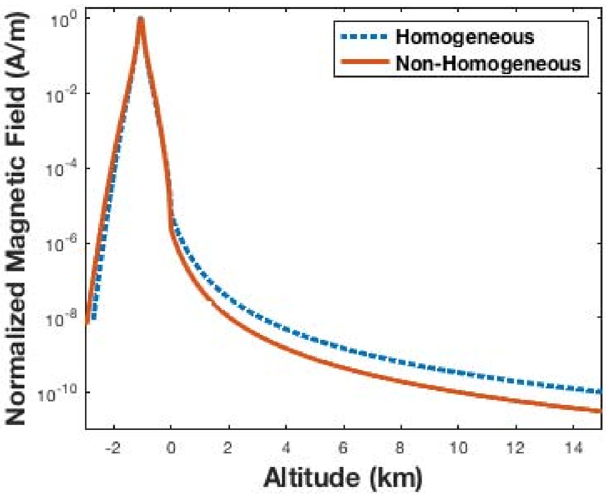

Fig. 12. Plot comparing the attenuation of the normalized magnetic field for a homogenous ocean to a nonhomogeneous ocean. The attenuation rate is faster for a nonhomogenous as the ocean has a higher conductive value toward the ocean surface.

substantially influence the fields in the ocean region, and the magnetic fields below the ocean–air interface are nearly the same in Model #2 as they are in Model #1 when no air region is included. This is because any fields that are reflected straight back down toward the source are strongly attenuated as they propagate. The reflected fields are very small relative to the direct fields from the source.

X. Ocean Salinity

The conductivity of the ocean changes with depth as well as with other factors. The temperature and pressure of the ocean change the mobility of hydrated ions of the dissolved salts [18]. The salinity of the ocean in turn affects the electrical conductivity of the ocean between shallow and deep water making the ocean a nonhomogeneous material. In colder deep ocean water, the conductivity is ~2.5 S/m, and in warmer surface ocean water, the conductivity is ~6 S/m [18].

An advantage of FDTD is that it can account for the spatially varying salinity within the ocean. Model #2 (the ocean–ionosphere) is a rerun assuming a hypothetical scenario of varying ocean water electrical conductivity since the actual variation of the ocean conductivity is not known and can change depending on the location. The conductivity is set to $\sigma = 3.3$ S/m at the location of the source. It remains constant below the source and linearly increases above the source. At an altitude of 1 km above the source (at the ocean surface), the conductivity is 6 S/m. The results are presented in Fig. 12.

Accounting for temperature variations of the ocean water results in a slightly increased attenuation of the magnetic field since the average conductivity is higher for the inhomogeneous case than for the homogeneous case. Another difference between the two results is at the ocean–air interface. The amplitude is shifted down for the nonhomogeneous case compared to the homogeneous case because the contrast of the conductivity across the interface is higher (material conductivity change of 6 S/m to air/free space versus 3 S/m to air). The evanescent wave above the ocean surface has lower amplitude for the nonhomogeneous case.

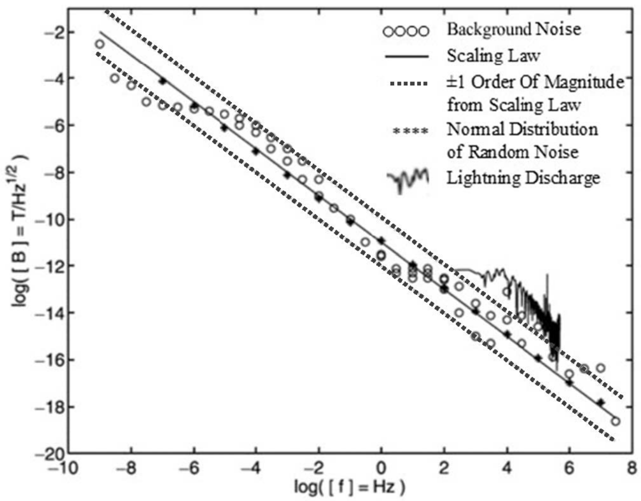

Fig. 13. Measured magnetic field spectrum of the background noise from $\sim 10^{-9}$ to $\sim 10^{7}$ Hz (circles) which can be approximated by the scaling law (solid line) $B = B_0(f_0/f)$ where $B_0 \approx 10^{-11}$ T/Hz$^{1/2}$, $f_0 = 1$ Hz is a scaling constant, and f is the frequency of the magnetic field. The measured magnetic field exhibits the deviations from the scaling law by $\sim\pm 1$ order of magnitude across the entire frequency range (dotted lines). The scaling law is simulated in the frequency range from 10^{-7} to 10^{7} Hz with a persistent normal distributed random noise process (stars) and exhibits an excellent agreement with the scaling law. The noisy solid line is measured data from a lightning discharge (courtesy of [19]).

XI. Background ULF Noise

Knowing the background noise level of ULF waves in the earth–ionosphere waveguide is helpful in understanding whether the scatterings from a submerged aircraft may be detectable at or above the ocean surface. From Fig. 2, the downward propagating electric/magnetic field drop to a depth of 1 km is less than 10:1 at 0.1 Hz. Then, from Fig. 5, the drop of the upward propagating FDTD-calculated magnetic field back up to the ocean surface is ~1000:1 at 0.1 Hz. Adding these together, there is a total magnetic field drop of 10 000:1 for the round-trip propagation.

Fig. 13 shows the background noise level over a wide range of frequencies for the magnetic field in the earth–ionosphere waveguide environment [19]. The experimental data are plotted along with a fitting curve. The highest magnetic field background noise level at 0.1 Hz is ~1E−9 T/Hz$^{1/2}$. Assuming a 0.1 Hz receiver bandwidth, the background level is 0.316 nT. To generate a detectable signal, the ULF transmitter would need to generate an impinging magnetic field of 3.16 μT at the ocean surface (assuming a 10 000:1 total drop of the magnetic field). A narrower receiver bandwidth could be used, which would lengthen the time needed to detect the signal. However, a narrower receiver bandwidth would permit an ULF transmitter to generate a smaller amplitude magnetic field at the ocean surface.

XII. Subtracting the Incident Waveform

In Section I, the proposed ULF radar system is described as being a three-step process. The results in Sections II–X indicate that the amplitude of the scattered fields from the aircraft will be well below the incident EM field amplitudes directly from the ULF source. In general, there are two possibilities for subtracting out the incident source values in order to obtain the scattered fields from the target: 1) subtraction based on the previous measurements obtained before the airplane presents in the region of interest and 2) using gradiometry to estimate the variation of the incident fields in the region of interest.

For 1), when using a stationary source such as HAARP background source fields (with no submerged aircraft) could be established by taking measurements in the regions of interest while the source is on but before the airplane is submerged in the ocean. Such baseline values could be obtained for different times of day, etc. Later, after an aircraft submerges into the ocean, taking new measurements in the vicinity of the crash site could be subtracted from the previously established baseline values to obtain the subtracted (scattered) EM fields from the target of interest.

Regarding 2), a general EM gradiometer is comprised two oppositely wound coils on ferrite rods separated by a "small" distance. These two coils on ferrite rods form a magnetic dipole antenna array. For many applications, such as those discussed in [20], the coils would be relatively close (as shown in [20, Fig. 4]). However, for the application discussed in this paper, the wavelength at ULF is longer than the circumference of the earth, so the ferrite rods might be kilometers or perhaps tens of kilometers apart. (The exact distance between the coils would depend on the location of interest, such as proximity to land, and will be investigated further as part of future research.) Note that in our case, the gradiometers would be used to estimate the variation of the source (incident) fields on the ocean, rather than to obtain the scattered waves from the target of interest (which would be measured via a highly sensitive magnetometer). For example, referring to Fig. 9, if the two coils of the gradiometer are outside the region where the primary scatterings from the target exist, such as having one coil at −10 km and the other coil at +10 km, the variation of the ULF source fields in the earth–ionosphere waveguide may be obtained by estimating a linear variation between the two coils (over the 20 km distance between the two coils). This gradiometer approach would be needed if baseline values were not previously obtained, or if it is believed that there was a significant change to the baseline values (such as during solar storms).

We note that Stolarczyk *et al.* [20] state that as of 2005, EM gradiometry had undergone extensive developments to improve the system sensitivity and to allow for the use of stand-off transmitters. Stolarczyk *et al.* [20] also suggests that synchronizing the gradiometers with the source can improve the detection capabilities, as well as taking measurements at different frequencies. For the application discussed in this paper, the choice of multiple frequencies would depend on the depth of the source.

XIII. Conclusion

Improved technology is needed to accurately detect the presence of objects such as aircrafts within the oceans. A global ULF detection system was proposed that involves generating a worldwide ULF EM field that penetrates into every ocean. Baseline ULF EM field values would be compared to perturbations of ULF EM fields generated by the objects of interest submerged at depths at points of interest in order to detect the objects in the real time.

Plane-wave theory and FDTD calculations in this paper indicate that ULF scatterings from objects may be detectable above the background noise at or above the ocean surface. ULF EM waves have the capability to propagate globally with negligible attenuation in the earth–ionosphere waveguide. Refraction at the air/ocean interface yields a downward ULF plane wave that attenuates according to the plane wave theory. This results in a magnetic field drop off to a depth over 1 km of less than 10:1 at 0.1 Hz. FDTD was then used to calculate a magnetic field drop of 1000:1 at 0.1 over the distance back up to the ocean surface. Taking both of these together, the total magnetic field drop is 10 000:1. Assuming a 0.1 Hz receiver bandwidth, a ULF transmitter would need to generate an impinging magnetic field of 3.16 μT at the ocean surface in order for the scatterings to be detectable above the magnetic background noise level of 0.316 nT.

The proposed radar system and results in this paper are notably different from that of [4] in many respects. For example, in this paper, FDTD provided rigorous Maxwell's equation solutions of the scatterings from the aircraft. In [4], assumptions and simplifications were required to make the analytical calculations solvable. Next, in this paper, the proposed ULF detection system involves a remote ULF source which generates the EM fields capable of penetrating every ocean to greater depths (on the order of 1 km). In [4], localized ELF detections to 100 m were discussed, and the transmitter and receiver would have to relocated to every position of interest. Finally, in this paper, the effects of the ocean floor and ionosphere were shown to be more insignificant in the FDTD results at ULF than assumed in [4].

Acknowledgment

Computing resources were primarily provided by the Department of Defense through the High Performance Computing Modernization Program. The authors would like to thank the Center for High Performance Computing, University of Utah, Salt Lake City, UT, USA, for providing supercomputing resources. Approved for public release, distribution unlimited.

References

[1] J. Sudworth, "Flight MH370 'Crashed in South Indian Ocean'-Malaysia PM," BBC News, London, U.K., Tech. Rep. 26716572, 2014.
[2] J. Sudworth, "New missing Malaysian plane MH370 search area announced," BBC News, London, U.K., Tech. Rep. 28031741, 2014.
[3] T. R. Clem, "Superconducting magnetic gradiometers for underwater target detection," *Nav. Eng. J.*, vol. 110, no. 1, pp. 139–149, Jan. 1998.
[4] R. W. P. King, "Lateral electromagnetic waves from a horizontal antenna for remote sensing in the ocean," *IEEE Trans. Antennas Propag.*, vol. 37, no. 10, pp. 1250–1255, Oct. 1989.

[5] A. McLeish, “Planet Earth,” in *Geological Science*, 2nd ed. Cheltenham, U.K.: Thomas Nelson Sons, 1992, p. 6.
[6] A. V. Streltsov and T. R. Pedersen, “An alternative method for generation of ULF waves by ionospheric heating,” *Geophys. Res. Lett.*, vol. 37, Jul. 2010, Art. no. L14101.
[7] A. V. Streltsov, C.-L. Chang, J. Labenski, G. Milikh, A. Vartanyan, and A. L. Snyder, “Excitation of the ionospheric Alfvén resonator from the ground: Theory and experiments,” *J. Geophys. Res., Space Phys.*, vol. 116, Jul. 2011, Art. no. A10221.
[8] P. T. I. Eriksson, L. G. Blomberg, S. Schaefer, and K.-H. Glassmeier, “On the excitation of ULF waves by solar wind pressure enhancements,” *Ann. Geophys.*, vol. 24, pp. 3161–3172. Nov. 2006.
[9] S. G. Claudepierre, S. R. Elkington, and M. Wiltberger, “Solar wind driving of magnetospheric ULF waves: Pulsations driven by velocity shear at the magnetopause,” *J. Geophys. Res., Space Phys.*, vol. 113, May 2008, Art. no. A05218.
[10] K. S. Yee, “Numerical solution of initial boundary value problems involving Maxwell’s equations in isotropic media,” *IEEE Trans. Antennas Propag.*, vol. AP-17, no. 3, pp. 302–307, May 1966.
[11] A. Taflove and S. Hagness, “Electrodynamics entering the 21st century,” in *Computational Electrodynamics: The Finite-Difference Time-Domain Method*, 3rd ed. Norwood, MA, USA: Artech House, 2005, ch. 1, p. 1.
[12] P. R. Bannister, “ELF propagation update,” *IEEE J. Ocean. Eng.*, vol. JOE-9, no. 3, pp. 179–188, Jul. 1984.
[13] A. Taflove and S. C. Hagness, “Incident wave source conditions,” in *Computational Electrodynamics: The Finite-Difference Time-Domain Method*, 3rd ed. Norwood, MA, USA: Artech House, 2005, ch. 5, p. 220.
[14] A. Taflove and S. C. Hagness, “Numerical dispersion and stability,” in *Computational Electrodynamics: The Finite-Difference Time-Domain Method*, 3rd ed. Norwood, MA, USA: Artech House, 2005, ch. 4, p. 132.
[15] K. P. Spies and J. R. Wait, “Characteristics of the earth-ionosphere waveguide for VLF radio waves,” Nat. Bur. Standards, Boulder, Co, USA, Tech. Note 300, 1964.
[16] A. Taflove and S. Hagness, “Local subcell models of fine geometrical features,” in *Computational Electrodynamics: The Finite-Difference Time-Domain Method*, 3rd ed. Norwood, MA, USA: Artech House, 2005, ch. 1, p. 432.
[17] J. H. Beggs, R. J. Luebbers, K. S. Yee, and K. S. Kunz, “Finite-difference time-domain implementation of surface impedance boundary conditions,” *IEEE Trans. Antennas Propag.*, vol. 40, no. 1, pp. 49–56, Jan. 1992.
[18] S. Maus, “Electromagnetic ocean effects,” in *Encyclopedia of Geomagnetism and Paleomagnetism*. New York, NY, USA: Springer, 2007, pp. 740–742.
[19] M. Füllekrug and A. C. Fraser-Smith, “The Earth’s electromagnetic environment,” *Geophys. Res. Lett.*, vol. 38, Nov. 2011, Art. no. L21807, doi: 10.1029/2011GL049572.
[20] L. G. Stolarczyk, R. Troublefield, and J. Battis, “Detection of underground tunnels with a synchronized electromagnetic wave gradiometer,” *Proc. SPIE*, vol. 5778, pp. 994–1001, May 2005, doi: 10.1117/12.609623.

Dallin R. Smith (S’16) received the B.Sc. degree in physics from Brigham Young University, Provo, UT, USA, in 2016. He is currently pursuing the Ph.D. degree with the Electrical and Computer Engineering Department, University of Utah, Salt Lake City, UT, USA.

His current research interests include modeling electromagnetic wave propagation with the finite-difference time-domain method.

Mr. Smith was a recipient of the William G. Holt Graduate Fellowship.

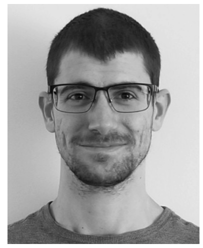

Sean Burns received the B.S. degree in mathematics and physics from the University of Utah, Salt Lake City, UT, USA, where he is currently pursuing the Ph.D. degree in electrical and computer engineering.

His current research interests include finite-difference time-domain modeling of very low-frequency radio waves in the earth–ionosphere waveguide running on supercomputers.

Jamesina J. Simpson (S’01–M’07–SM’12) received the B.S. and Ph.D. degrees in electrical engineering from Northwestern University, Evanston, IL, USA, in 2003 and 2007, respectively.

She is currently an Associate Professor with the Electrical and Computer Engineering Department, University of Utah, Salt Lake City, UT, USA. Her research lab encompasses the application of the Maxwell equation finite-difference time-domain method to a wide variety of scientific and engineering applications across the electromagnetic spectrum.

Dr. Simpson received the 2010 NSF CAREER Award, the 2012 Donald G. Dudley, Jr. Undergraduate Teaching Award of the IEEE Antennas and Propagation Society, and the 2017 International Union of Radio Science Santimay Basu Medal.

Stephanie M. Ferrone received the B.S. degree from the University of Maryland–Baltimore County, Baltimore, MD, USA, in 2009, and the M.S. degree from Johns Hopkins University, Baltimore, in 2014.

She is currently a Physicist and a Program Manager in underwater electromagnetic signatures and technology with the Carderock Division, Naval Surface Warfare Center, Arlington, VA, USA.